Iranian Journal of Basic Medical Sciences
ijbms.mums.ac.ir

Melatonin alleviates ferroptosis in lens epithelial cells via regulating METTL14 expression

Huirui Liu [1, 2], Fengchun Kang [1, 2], Junyao Lu [2], Jialin Luo [1, 2], Yi Gao [1, 2], Zijian Yu [1], Qi An [1], Chen Yang [1], Liyao Sun [1], Hongyan Ge [1*]

[1] Eye Hospital, The First Affiliated Hospital of Harbin Medical University, Harbin, China
[2] The Key Laboratory of Cardiovascular Disease Acousto-Optic Electromagnetic Diagnosis and Treatment in Heilongjiang Province, the First Affiliated Hospital, Harbin Medical University, Harbin, China

ARTICLE INFO

Article type:
Original

Article history:
Received: Nov 18, 2025
Accepted: Jul 1, 2026

Keywords:
Cataract
Epithelial cells
Ferroptosis
Lens crystalline
Melatonin
N6-methyladenosine
Oxidative stress
Ultraviolet rays

ABSTRACT

Objective(s): Ferroptosis in lens epithelial cells (LECs) is increasingly recognized as a key pathological process in cataract formation, driven by oxidative stress, lipid peroxidation, and aberrant RNA modification. This study investigated the role of METTL14 in UVB-induced ferroptosis in LECs and explored the protective mechanism of melatonin (MT).

Materials and Methods: mRNA and protein levels of METTL14 and ferroptosis-related markers (GPX4, SLC7A11) were quantified. Lipid reactive oxygen species (ROS), malondialdehyde (MDA), and glutathione levels were measured to assess ferroptotic activity. Mitochondrial structure and function were evaluated using transmission electron microscopy, mitochondrial membrane potential analysis, and ATP quantification. *In vitro*, METTL14 knockdown was achieved via siRNA in UVB-irradiated LECs. *In vivo*, a UVB-induced rat cataract model was used to assess lens opacity, histopathological changes, and ferroptosis-related protein expression.

Results: UVB irradiation significantly up-regulated METTL14 expression and promoted ferroptosis in LECs. MT treatment reduced METTL14 expression, suppressed ferroptosis *in vitro* and *in vivo*, alleviated lipid peroxidation, and restored mitochondrial morphology and function. In rats, MT markedly decreased lens opacity and attenuated UVB-induced pathological alterations.

Conclusion: MT inhibits METTL14-mediated ferroptosis in LECs, reduces lipid peroxidation, and restores mitochondrial function, thereby slowing cataract progression. These findings highlight METTL14 as a critical regulator of ferroptosis and support MT as a promising therapeutic strategy for cataract prevention and treatment.

▶ Please cite this article as:
Liu H, Kang F, Lu J, Luo J, Gao Y, Yu Z, An Q, Yang C, Sun L, Ge H. Melatonin alleviates ferroptosis in lens epithelial cells via regulating METTL14 expression. Iran J Basic Med Sci 2026; 2

Introduction

Cataract is the leading cause of blindness worldwide (1), and it is caused by various factors such as aging, genetics, ultraviolet exposure, smoking, and diabetes (2, 3). Currently, surgical removal of the cloudy lens and implantation of an artificial lens are the only effective treatment methods, but their complications and high costs limit their clinical application (4). Therefore, there is an urgent need to explore new drug intervention strategies.

Existing studies generally suggest that damage to lens epithelial cells (LECs) is the initiating link in cataract formation, mediated by mechanisms including apoptosis, necrosis, senescence, ferroptosis, autophagy, and oxidative stress (5-7). In recent years, ferroptosis, as a non-apoptotic cell death mode dependent on iron ions, has been confirmed to be closely related to the occurrence and development of cataract (8, 9). Its morphological characteristics include reduced cell volume and increased membrane density, while its biochemical features are the accumulation of iron-dependent lipid peroxidation (10, 11). Under normal circumstances, the body maintains a dynamic balance through the iron-ROS oxidation system and the Xc-/GSH/GPX4 antioxidant system; once the balance is disrupted, it may trigger ferroptosis and accelerate the pathological process of cataract (12).

Epigenetic modifications, especially m6A (N6-methyladenosine) modifications, have increasingly been shown to play important roles in cellular homeostasis and disease occurrence in recent years. m6A is the most common post-transcriptional modification form of eukaryotic mRNA (13, 14), and its "writer" complex is mainly composed of METTL3, METTL14, and WTAP. Although METTL14 lacks catalytic activity, it plays a key role in maintaining complex stability and target RNA recognition (15, 16). Studies have shown that METTL14 expression is abnormal in LECs from cataract patients, resulting in decreased m6A modification levels in circRNAs, which may contribute to the occurrence and development of cataract (17). In addition, METTL14 can affect the activity of the ferroptosis pathway by regulating the m6A modification levels of

*Corresponding author: Hongyan Ge. Eye Hospital, The First Affiliated Hospital of Harbin Medical University, Harbin, China. Email: gehongyan@hrbmu.edu.cn

ferroptosis-related genes (such as ACSL4 and SLC7A11) (18). This discovery provides new evidence for the cross-regulation between ferroptosis and m6A modification.

Melatonin (MT) has attracted widespread attention due to its significant antioxidant and cell-protective effects. MT is an indole hormone secreted by the pineal gland and participates in various physiological functions, including regulation of sleep rhythms, immune responses, and neuroprotection. Studies have shown that in human lens epithelial cells (HLECs), MT can inhibit H2O2-induced ROS generation and cell death by activating the PI3K/AKT signaling pathway, thereby exerting antioxidant and cell-protective effects (19). Although there is no completely safe and effective clinical application scheme for MT yet, it has shown potential therapeutic value in preventing UVB-induced cataract (20).

We therefore aimed to investigate the therapeutic effects and molecular mechanisms of MT in cataract formation. MT attenuated lens opacity by suppressing ferroptosis in LECs through down-regulation of METTL14 and restoration of mitochondrial function. Our findings provide new insights into the role of METTL14-mediated ferroptosis in cataract pathogenesis and suggest MT as a promising therapeutic strategy to delay or prevent cataract progression.

Materials and Methods

Rat model of cataract

Six-week-old male Sprague-Dawley (SD) rats were acquired from the Experimental Animal Center of the Second Affiliated Hospital of Harbin Medical University and housed in the Department of Experimental Animals at Harbin Medical University. All animal procedures followed the ARVO Statement for the Use of Animals in Ophthalmic and Vision Research and were approved by the Animal Ethics Committee of the First Affiliated Hospital of Harbin Medical University (Approval No. 2023130). The rats were anesthetized via intraperitoneal injection of a mixture of ketamine (90 mg/kg) and xylazine (15 mg/kg), and topical proparacaine hydrochloride eye drops were applied before ocular manipulation for local ocular anesthesia. No additional analgesic was administered because the UVB-induced cataract model was established under general and local ocular anesthesia and did not involve surgical incision. Tropicamide-phenylephrine eye drops were then applied to both eyes, and the rats that underwent drug treatment received subconjunctival injections of 25 µl/eye with either 500 mM Fer-1, 200 mM MT (HY-B0075; MCE, USA), or an equivalent volume of DMSO (used as the drug solvent). After a 5-minute waiting period, only the right eye of each rat was exposed to UVB radiation for 15 minutes using a handheld UV lamp (LUYOR LEB-280 L, USA) emitting at 312 nm, delivering a dose of 0.45 J/cm², measured by a UVB sensor (TM-213, Tenmars, China)(7). This irradiation was administered daily for seven consecutive days. Upon completion of the experiment, the rats were euthanized by CO_2 asphyxiation. The lens was carefully extracted via a posterior approach under sterile conditions and fully separated along its edge.

Cell Culture

The human lens epithelial cell line SRA01/04 (Procell system, China) was cultured in Dulbecco's Modified Eagle Medium (DMEM) supplemented with 10% fetal bovine serum (FBS) and 1% penicillin-streptomycin at 37 ˚C in a humidified incubator with 5% CO_2. Cells were maintained in 10% FBS and used for experiments when they reached 70% confluence in the logarithmic growth phase. The irradiation times were 0s, 20s, 40s, 100s, 120s, 160s, 200s, 240s and 300s respectively, to obtain UVB doses of 0J/m², 100J/m², 200J/m², 500J/m², 600J/m², 800J/m², 1000J/m², 1200J/m² and 1500J/m², which were measured using a calibrated UVB radiation meter. The effective UVB dose range that ensures at least a 50% cell survival rate was selected and will be used in subsequent experiments. For specific treatments, HLECs were pretreated with 250 µM MT for 24 hours, then incubated in culture medium with or without UVB irradiation for 24 hours.

siRNA transfection

HLECs were seeded in six-well plates and cultured until they reached approximately 60% confluence. The cells were then transfected with METTL14-specific siRNA or negative control siRNA (siNC)(GenePharma, Shanghai, China) using Lipofectamine 2000 (Invitrogen, USA) according to the manufacturer's instructions. Briefly, siRNAs and Lipofectamine 2000 were each diluted in serum-free DMEM, gently mixed, and incubated at room temperature for 20 minutes to form transfection complexes. The complexes were then added to the cells. Six hours after transfection, the medium was replaced with fresh DMEM containing 10% FBS, and the cells were cultured for an additional 24 hours before subsequent experiments.

Cell counting Kit-8 (CCK-8) assay

The cells were inoculated into 96-well plates, gently agitated, and then placed in the incubator for 24 hours of static incubation. Subsequently, different doses of UVB irradiation were carried out. Each group was set with 5 replicate wells to enhance the reliability of the experimental results. After 24 hours in each well, 100 µl of complete medium was added and mixed with 10 µl of CCK-8 solution (SC119, Seven, China). It was then immediately placed in the cell incubator for 1 hour. The OD value at wavelength 450 nm of each group was measured using an enzyme detector (SpectraMax Mini Reader, Molecular Devices, USA).

Quantitative real-time polymerase chain reaction (qRT-PCR)

Total RNA was isolated from treated cells using the Total RNA Extraction Kit (BSC52M1; BioFlux, USA) and subsequently reverse-transcribed into cDNA using a reverse transcription kit (SM134-02; Seven, China). qRT-PCR was conducted using SYBR Green Master Mix (G3326; Servicebio, China) to assess gene expression levels. The relative mRNA expression was analyzed using the $2^{-\Delta\Delta Ct}$ method. The primer sequences are shown in Table 1 (21).

Western blot analysis (WB)

Total protein was extracted from HLECs using RIPA buffer containing 1 mM PMSF, followed by centrifugation at 12,000 rpm for 15 minutes to remove debris. Equal amounts of protein were separated by SDS-PAGE and transferred to polyvinylidene fluoride membranes. After blocking with 5% skim milk at room temperature for 1 hour, membranes were incubated with primary antibodies at 4 ˚C overnight. The primary antibodies are shown in Table 2. Following

Table 1. Gene-specific primer sequences used for quantitative real-time PCR (qRT-PCR) in this study

Gene	Primer sequences
METTL14-F	5′-GTAGCACAGACGGGGACTTC-3′
METTL14-R	5′-AGGCGTCTTCTACCAAGACAA-3′
GPX4-F	5′-CGATACGCTGAGTGTGGTTT-3′
GPX4-R	5′-CGGCGAACTCTTTGATCTCTT-3′
SLC7A11-F	5′-GGTTGCCCTTTCCCTCTATTC-3′
SLC7A11-R	5′-CCTGGGTTTCTTGTCCCATATAA-3′
GAPDH-F	5′-GTGGTCTCCTCTGACTTCAACA-3′
GAPDH-R	5′-CTCTTCCTCTTGTGCTCTTGCT-3′

METTL14: Methyltransferase-like 14; GPX4: Glutathione peroxidase 4; SLC7A11: Solute carrier family 7 member 11; GAPDH: Glyceraldehyde-3-phosphate dehydrogenase

three washes with TBST, membranes were probed with HRP-conjugated secondary antibodies and visualized using an enhanced chemiluminescence detection system (Champchemi, SINSAGE, China). Band intensities were quantified using ImageJ software (22).

Hematoxylin and eosin (HE) staining

The rat eyeballs were fixed in Davidson's fixative, dehydrated, and then embedded in paraffin. First, the nuclear material was stained using hematoxylin solution (G1120, Solarbio, China). Next, the sample was rinsed with running tap water, and then the cytoplasm was counterstained with eosin. Finally, images were captured using a microscope (7).

Immunohistochemical (IHC) staining

Rat eyeballs were fixed in Davidson's solution, dehydrated, and embedded in paraffin. After sectioning, deparaffinization, and microwave antigen retrieval, endogenous peroxidase was quenched with 3% H_2O_2, followed by blocking with 5% BSA for 1 hr. Sections were incubated with primary antibodies overnight at 4 ˚C and then with a two-step mouse/rabbit secondary antibody system for 1 hr at room temperature. Immunoreactivity was detected using DAB, and sections were dehydrated, cleared, and imaged under a light microscope.

Table 2. Information on antibodies used for Western blot (WB) in this study

Antibody name	Dilutions	Vendor name	Cat No.
METTL14	1:2000	Proteintech	26158-1-AP
GPX4	1:2000	Abcam	ab262509
SLC7A11	1:10000	Proteintech	10442-1-AP
GAPDH	1:2000	OriGene	TA802519

METTL14: Methyltransferase-like 14; GPX4: Glutathione peroxidase 4; SLC7A11: Solute carrier family 7 member 11; GAPDH: Glyceraldehyde-3-phosphate dehydrogenase

Immunofluorescence (IF) assay

The processed cells were collected, fixed, permeabilized, and blocked. Subsequently, the cells were incubated with the first antibody (1:100, METTL14) at 4 ˚C overnight, then with the second antibody (1:100, goat anti-rabbit [ZF-0316, ZSGB-BIO] and anti-mouse [ZF-0313, ZSGB-BIO]) at room temperature for 1 hour, and finally stained with DAPI. Finally, images were obtained using the Zeiss fluorescence microscope system (Vert.A1, Zeiss, Germany). All IF images from different groups were acquired under identical exposure and gain settings. For each sample, at least three randomly selected fields from three independent experiments were imaged. The mean fluorescence intensity was quantified using ImageJ software after background subtraction and normalized to the control group's fluorescence intensity (23).

ROS measurement

The intracellular ROS levels were measured using dihydroethidium (DHE) (HY-D0079, MCE, USA). The cells were co-incubated with 5 μM DHE for 30 minutes at 37 ˚C and then imaged using a fluorescence microscope (Vert.A1, Zeiss, Germany). The results were analyzed using ImageJ (version 2.1.0/1.53c).

Mitochondrial membrane potential (MMP)

To detect mitochondrial membrane potential (MMP), JC-1 (C2003S; Beyotime, China) was used. Cells were incubated with the JC-1 probe at 37 ˚C for 40 minutes. Imaging was performed using a microscope (IX73, Olympus, Japan) (24).

Molecular docking

The structures of drugs and key target proteins were obtained from the PubChem database (https://pubchem.ncbi.nlm.nih.gov) and the PDB database (https://www.rcsb.org). Visualization was performed using PyMOL software.

Transmission electron microscopy (TEM)

These cells were fixed with 2.5% glutaraldehyde. Subsequently, the cells were washed with PBS solution and fixed with 1% osmium tetroxide for 1 hour. After ethanol dehydration treatment, the samples were embedded in epoxy resin. Then, an experienced pathologist used an H-7700 transmission electron microscope (Hitachi High Technology Corporation, Tokyo, Japan) to acquire images at an accelerating voltage of 100 kilovolts (25).

Measurement of oxidative stress markers

Cells were treated with thiobarbituric acid, and the level of MDA (BC0025; Beyotime, China) was determined by colorimetric analysis (at wavelengths of 532 nanometers and 600 nanometers). To determine the antioxidant status in LECs after UVB exposure, intracellular GSH (S0053; Beyotime, China) was measured. GSH activity was determined by reacting GSH with dithiobenzoic acid. The absorbance was measured at 412 nanometers to determine the GSH activity.

ATP measurement

Cellular ATP levels were measured using a commercial ATP assay kit (HY-D0079; Beyotime, China) following the manufacturer's instructions. In brief, cells were lysed and

centrifuged at 12,000 × g for 5 min at 4 ˚C, and the resulting supernatant was transferred to a black 96-well plate containing the ATP working solution. Chemiluminescence was then recorded using a SpectraMax MiniReader (Molecular Devices, USA), and ATP content was quantified accordingly (26).

Statistical analysis

All experiments were independently repeated at least three times. Data are presented as mean±standard error (SEM). Statistical analysis was performed using GraphPad Prism 9 software. For normally distributed data, comparisons between two groups were performed using Student's *t*-test, and comparisons among multiple groups were performed using one-way ANOVA. *P-values*<0.05 were considered statistically significant (*P<0.05, **P<0.01, ***P<0.001, ****P<0.0001).

Results

Ferroptosis was induced in LECs via dose-dependent UVB exposure

To determine the optimal UVB irradiation dose that LECs could tolerate, we exposed cells to a UVB dose gradient and assessed cell viability using the CCK-8 assay.

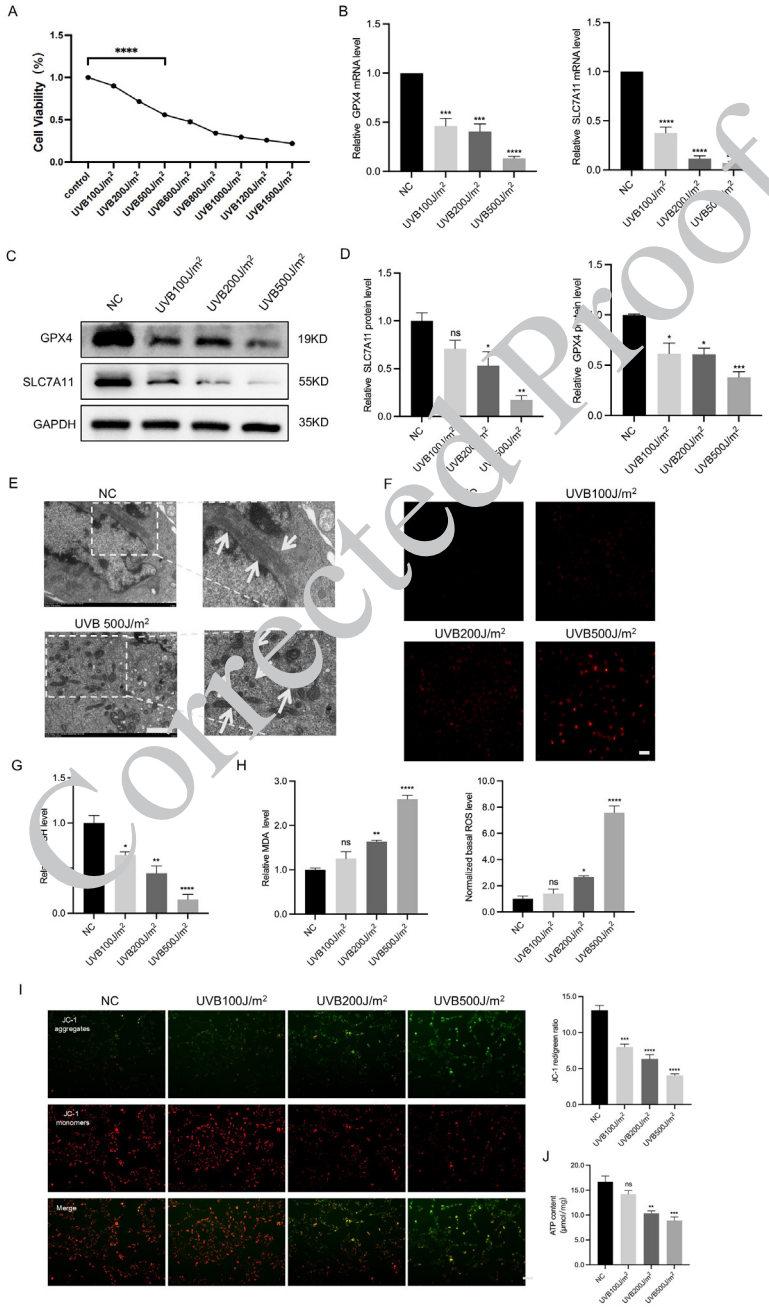

Figure 1. Ferroptosis was induced in rat lens epithelial cells (LECs) via dose-dependent ultraviolet B (UVB) exposure
(A) Cell Counting Kit-8 (CCK-8) assay results for LECs after UVB irradiation. (B) The mRNA expression levels of GPX4 and SLC7A11 at UVB doses of 0 J/m², 100 J/m², 200 J/m² and 500 J/m². (C, D) The protein expression levels of GPX4 and SLC7A11 at UVB doses of 0 J/m², 100 J/m², 200 J/m² and 500 J/m². (E) Mitochondrial ultrastructure was observed by transmission electron microscopy (TEM). Scale bar=2 μm. (F) Intracellular reactive oxygen species (ROS) levels were detected using dihydroethidium (DHE) staining. Scale bar=200 μm. (G, H) Analyze the expression levels of oxidative stress markers in LECs. (I) Mitochondrial membrane potential (MMP) was measured by JC1 staining. Scale bar=100 μm. (J) Adenosine triphosphate (ATP) levels were quantified in each group. *P<0.05; **P<0.01; ***P<0.001; ****P<0.0001. Data are shown as mean±SEM (n=3)
GPX4: Glutathione peroxidase 4; SLC7A11: Solute carrier family 7 member 11; GSH: Glutathione; MDA: Malondialdehyde; NC: Negative control; SEM: standard error of mean

As shown in Figure 1A, LEC viability declined progressively with increasing UVB intensity (0, 100, 200, 500, 600, 800, 1000, 1200, and 1500 J/m²). Considering that 500 J/m² preserved approximately 50% cell viability while inducing evident ferroptosis-related changes, this dose was selected as a sublethal injury dose for subsequent mechanistic experiments. Higher doses were not used in subsequent experiments to avoid excessive nonspecific cytotoxicity. At the molecular level, the ferroptosis-related markers GPX4 and SLC7A11 exhibited dose-dependent decreases in both mRNA and protein expression following UVB exposure (Figure 1B, C, D). TEM further revealed that, compared with the control group, LECs subjected to UVB displayed shrunken mitochondria with increased membrane density and reduced cristae volume, while nuclear morphology remained largely unaltered (Figure 1E). Consistent with ferroptotic features, UVB irradiation induced excessive accumulation of ROS, as indicated by increased DHE fluorescence intensity (Figure 1F). In addition, oxidative stress markers were significantly altered: GSH levels were reduced, whereas MDA levels were elevated in UVB-treated cells (Figure 1G, H). UVB exposure also led to a pronounced reduction in mitochondrial membrane potential (MMP), as evidenced by JC-1 staining (Figure 1I). Finally, intracellular ATP levels decreased in a dose-dependent manner upon UVB treatment (Figure 1J).

Expression of METTL14 in LECs under UVB irradiation

To investigate the expression of METTL14 in LECs after UVB exposure, we first measured its mRNA level and observed persistent up-regulation relative to the control group (Figure 2A). Additionally, WB analysis revealed that METTL14 protein expression increased significantly after 500 J/m² of UVB irradiation (Figure 2B, C). IF staining further confirmed these results, indicating that METTL14 expression increased significantly in response to UVB stimulation. In summary, these results suggest that UVB exposure significantly up-regulates METTL14 expression in LECs.

Knocking down METTL14 reduced UVBinduced LECs ferroptosis

To investigate the role of METTL14 in UVB-induced ferroptosis in LECs, we established a METTL14 knockdown model *in vitro* and performed functional loss experiments (Figure 3A). The results showed that siRNA#2 and #3 exhibited the highest interference efficiency, reducing the METTL14 mRNA level by more than 80% (Figure 3B). After UVB irradiation, METTL14 expression in LECs increased significantly, and METTL14 knockdown effectively reversed this up-regulation (Figure 3C, D). Regarding oxidative stress, UVB irradiation significantly increased intracellular ROS levels, whereas METTL14 knockdown significantly reduced ROS accumulation (Figure 3E). Further examination of mitochondrial function revealed that UVB irradiation led to decreased ATP levels and MMP, and that METTL14 knockdown could reverse these effects (Figure 3F, G). At the same time, the key regulatory factors of ferroptosis, GPX4 and SLC7A11, were significantly down-regulated in response to UVB induction, and their mRNA and protein

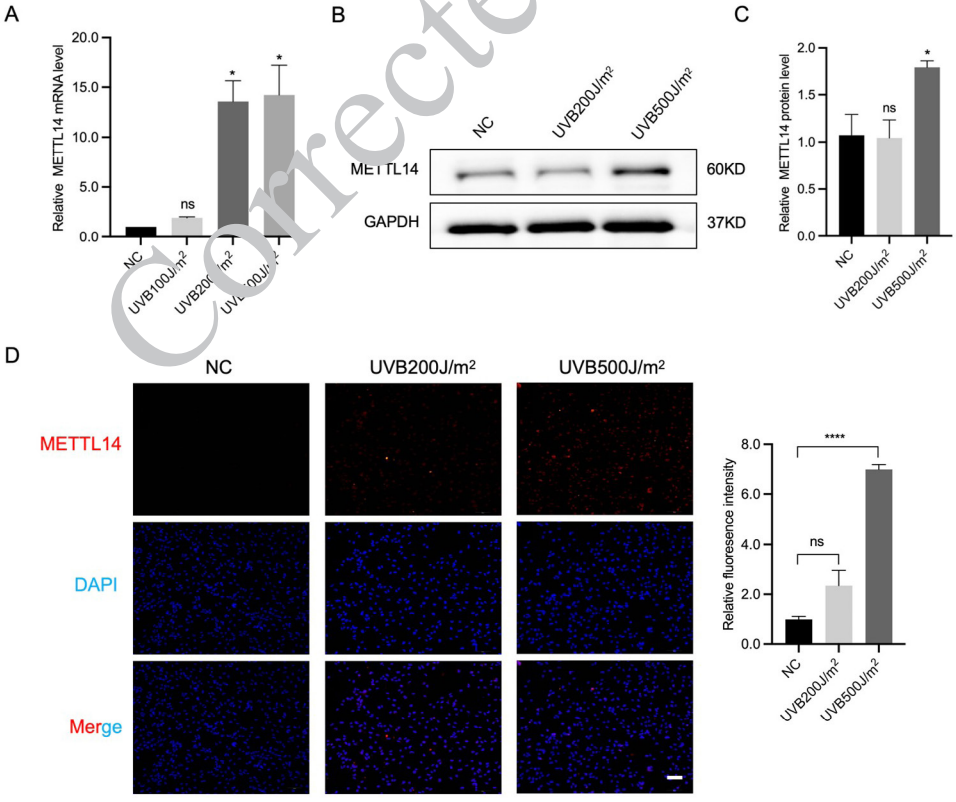

Figure 2. Ultraviolet B (UVB) irradiation induces up-regulation of METTL14 in rat lens epithelial cells (LECs)
(A) The mRNA expression level of METTL14 in LECs under UVB exposure. (B, C) Western Blot (WB) analysis of METTL14 protein expression in LEC with different UVB doses. (D) Immunofluorescence (IF) staining of METTL14 (red) merged with DAPI (blue) in each group. Scale bars=100 μm. *P<0.05; **P<0.01; ***P<0.001; ****P<0.0001. Data are shown as mean±SEM (n=3)
METTL14: Methyltransferase-like 14; NC: Negative control; SEM: standard error of mean

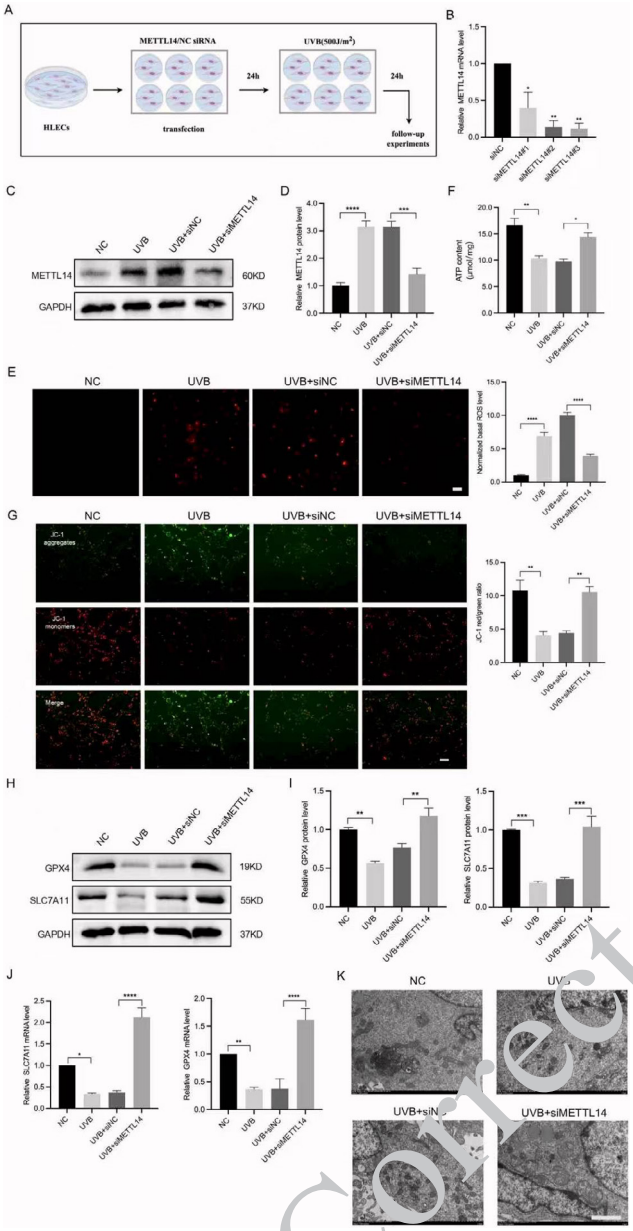

Figure 3. Knocking down METTL14 alleviated ultraviolet B (UVB)-induced ferroptosis in rat lens epithelial cells (LECs)
(A) The diagram of LECs culture and treatment. (B) METTL14 mRNA levels in LECs with different treatments. (C, D) METTL14 protein levels in LECs with different treatments. (E) Dihydroethidium (DHE) staining was used to detect the intracellular reactive oxygen species (ROS) levels in each group. Scale bar=200 μm. (F) Adenosine triphosphate (ATP) abundance levels in each group. (G) Mitochondrial membrane potential (MMP) was measured by JC1 staining. Scale bar=100 μm. (H, I, J) Western blot (WB) and quantitative real-time polymerase chain reaction (qRT-PCR) analyses of GPX4 and SLC7A11 in LECs treated with NC, UVB, UVB+siNC, and UVB+siMETTL14. (K) Results of transmission electron microscopy (TEM) when LECs were treated with NC, UVB, UVB+siNC, and UVB+siMETTL14. Scale bar=2 μm. $^{*}P<0.05$; $^{**}P<0.01$; $^{***}P<0.001$; $^{****}P<0.0001$. Data are shown as mean±SEM (n=3)
METTL14: Methyltransferase-like 14; GPX4: Glutathione peroxidase 4; SLC7A11: Solute carrier family 7 member 11; NC: Negative control; siNC: Negative control small interfering RNA; siMETTL14: METTL14 small interfering RNA; SEM: standard error of mean

expressions were restored after METTL14 knockdown (Figure 3H, I, J). The results of TEM observations further confirmed that the typical ultrastructural changes of ferroptosis, such as mitochondrial volume reduction, increased membrane density, and reduced cristae, were significantly improved after METTL14 knockdown (Figure 3K). These results suggest that knockdown of the METTL14 gene can effectively alleviate UVB-induced ferroptosis in LECs.

Melatonin inhibited UVB-induced ferroptosis in LECs

To verify whether UVB-induced cell damage is related to ferroptosis, we treated cells with the selective ferroptosis inhibitor Fer-1 and MT. The results showed that both could effectively alleviate UVB-induced cell damage (Figure 4A). Further analysis revealed that after treatment with Fer-1 or MT, the oxidative stress level in LECs exposed to UVB significantly decreased (Figure 4B, C, D). At the same time, compared with the simple UVB group, the expression levels of GPX4 and SLC7A11 in the Fer-1 group were significantly up-regulated, suggesting that the degree of ferroptosis in the cells was alleviated (Figure 4E, F). It is noteworthy that MT could also significantly increase the expression levels of GPX4 and SLC7A11 (Figure 4E, F). Compared with the UVB+DMSO group, the mitochondria of LECs treated with Fer-1 or MT returned to normal morphology (Figure 4G). Its effect was similar to that of Fer-1, suggesting that MT plays an important role in inhibiting UVB-induced ferroptosis.

Melatonin reduced METTL14 expression in LECs under UVB irradiation

The molecular docking results showed that MT bound to METTL14 via multiple hydrogen bonds and hydrophobic interactions, thereby stabilizing METTL14 within the

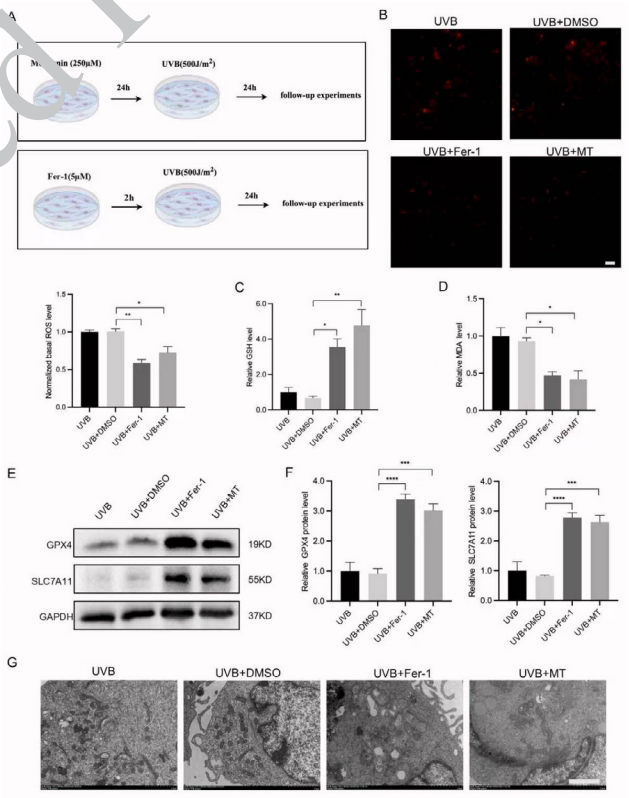

Figure 4. Melatonin (MT) inhibited ultraviolet B (UVB)-induced ferroptosis in rat lens epithelial cells (LECs)
(A) The LECs were treated with MT for 24 hr or with Fer-1 for 2 h. (B) Reactive oxygen species (ROS) were detected using the Dihydroethidium (DHE) dye. Scale bar=200 μm. (C, D) GSH and MDA levels in LECs with different treatments. (E, F) The results of Western blot (WB) analysis and the relative protein levels of GPX4 and SLC7A11 are shown. (G) Transmission electron microscopy (TEM) results in LECs treated in different ways. Scale bar=2 μm. $^{*}P<0.05$; $^{**}P<0.01$; $^{***}P<0.001$; $^{****}P<0.0001$. Data are shown as mean±SEM (n=3)
GPX4: Glutathione peroxidase 4; SLC7A11: Solute carrier family 7 member 11; DMSO: Dimethyl sulfoxide; Fer-1: Ferrostatin-1; GSH: Glutathione; MDA: Malondialdehyde; SEM: standard error of mean

protein-binding pocket and forming a stable complex (Figure 5A). To further verify the regulatory effect of MT on METTL14 in LECs, we treated the cells with MT-containing culture medium. The results showed that MT could significantly down-regulate the protein expression level of METTL14 in LECs (Figure 5B, C), and the IF results were consistent with the WB results (Figure 5D). Moreover, under UVB irradiation, MT effectively alleviated oxidative stress in LECs, as evidenced by a significant reduction in intracellular ROS levels (Figure 5E).

Melatonin regulated ferroptosis by targeting METTL14

To verify whether the regulatory effect of MT on ferroptosis in LECs depends on METTL14, we transfected LECs with siMETTL14 and treated them with MT in combination. The results showed that compared with the siMETTL14+DMSO group, the mRNA and protein expression levels of GPX4 and SLC7A11 in the siMETTL14+MT group were significantly up-regulated (Figure 6A, B, C). TEM observations further confirmed that the typical ultrastructural changes of ferroptosis (including reduced mitochondrial volume, increased membrane density, and decreased cristae) observed after siMETTL14 treatment were significantly improved with the addition of MT (Figure 6D). At the same time, mitochondrial function detection results indicated that MMP and ATP levels were restored under MT intervention, thereby alleviating the functional disorder induced by siMETTL14 (Figure 6E, F). Overall, these results suggest that MT can partially regulate ferroptosis in LECs by targeting METTL14, thereby exerting a protective effect on cells.

Melatonin restored lens transparency by suppressing ferroptosis

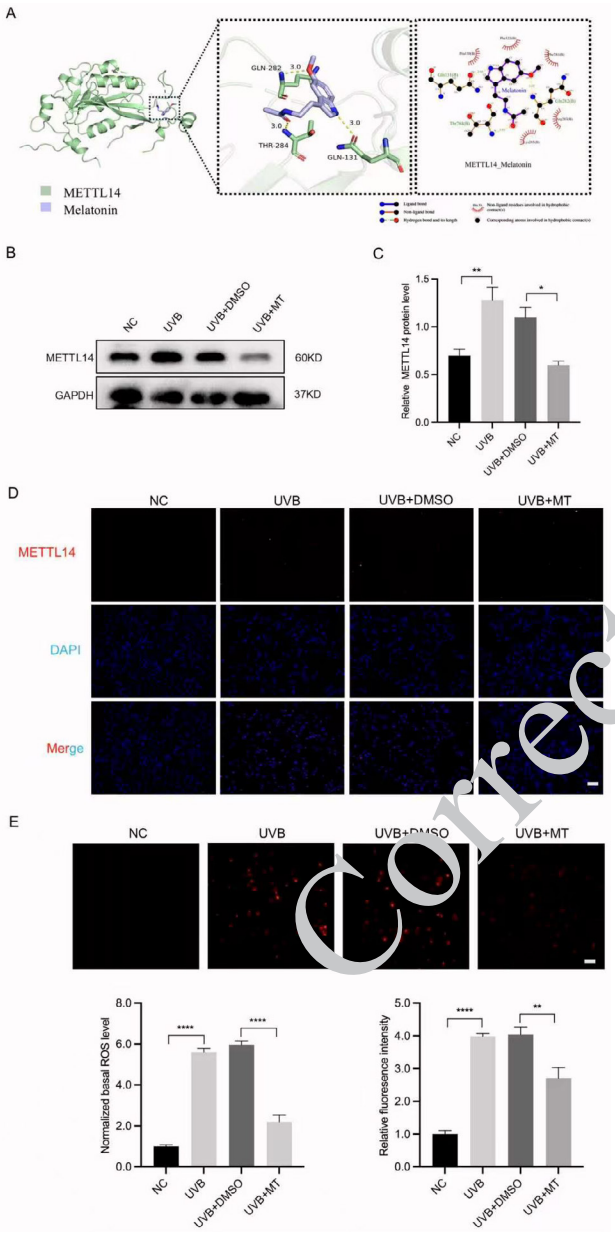

Figure 5. Melatonin (MT) reduced METTL14 expression in rat lens epithelial cells (LECs) under ultraviolet B (UVB) irradiation

(A) Schematic diagrams of the two-dimensional and three-dimensional structures of the MT-METTL14 interaction, with enlarged details. (B, C) Protein expression level of METTL14 with MT treatment. (D) Immunofluorescence (IF) staining of METTL14 (red) merged with DAPI (blue) in each group. Scale bar=100 μm. (E) Reactive oxygen species (ROS) were detected using the dihydroethidium (DHE) dye. Scale bar=200 μm. $^{*}P<0.05$; $^{**}P<0.01$; $^{****}P<0.0001$. Data are shown as mean±SEM (n=3) METTL14: Methyltransferase-like 14; NC: Negative control; DMSO: Dimethyl sulfoxide; SEM: standard error of mean

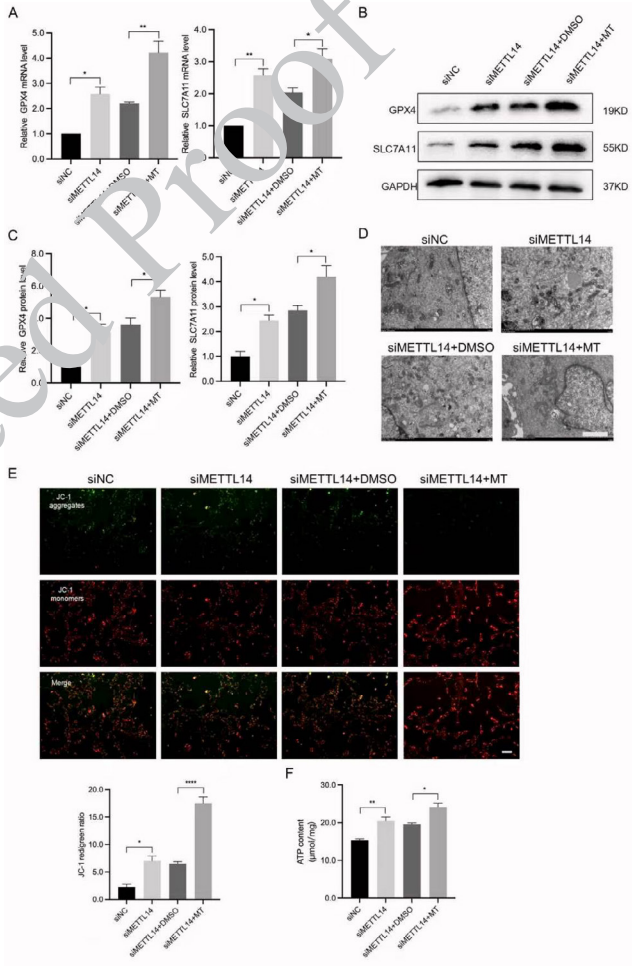

Figure 6. Melatonin (MT) regulates ferroptosis by targeting METTL14 in rats

(A) mRNA expression levels of GPX4 and SLC7A11 with MT treatment after transfection of siMETTL14. (B, C) Protein expression levels of GPX4 and SLC7A11 with MT treatment after transfection of siMETTL14. (D) Representative images of transmission electron microscopy (TEM) in LECs. Scale bar=2 μm. (E) Analysis of JC-1 stain in LECs. Scale bar=100 μm. (F) Analysis of adenosine triphosphate (ATP) in LECs. $^{*}P<0.05$; $^{**}P<0.01$; $^{****}P<0.0001$. Data are shown as mean±SEM (n=3)

METTL14: Methyltransferase-like 14; DMSO: Dimethyl sulfoxide; GPX4: Glutathione peroxidase 4; SLC7A11: Solute carrier family 7 member 11; siNC: Negative control small interfering RNA; siMETTL14: METTL14 small interfering RNA; SEM: standard error of mean

Based on *in vitro* results indicating that MT can inhibit UVB-induced ferroptosis and improve mitochondrial function, we further verified these effects in animal models. A cataract model was established using UVB irradiation (Figure 7A). The results showed that the lens in the DMSO control group remained transparent, whereas the UVB+DMSO group exhibited significant opacity. Notably, UVB combined with subconjunctival injection of ferroptosis inhibitor Fer-1 or MT significantly reduced lens opacity, presenting only scattered punctate opacity in the equatorial cortex of the lens and mild opacity of the epithelial cells (Figure 7B). The histological staining results further indicated that UVB irradiation caused significant pathological changes in the rat lens, including disordered arrangement of LECs, irregular cell gaps, vacuoles and swelling, as well as disordered proliferation and abnormal nuclear morphology (Figure 7C). However, MT or Fer-1 treatment effectively alleviated the above pathological damage, maintaining the relatively intact single-layer cubic arrangement structure of LECs (Figure 7C). Mechanistically, IHC results showed that UVB irradiation significantly increased METTL14 expression in the anterior capsule of the rat lens, whereas MT treatment significantly inhibited this increase (Figure 7D). At the same time, WB detection results showed that UVB irradiation decreased the expression levels of the ferroptosis-related markers GPX4 and SLC7A11 in the anterior capsule of the lens, and MT or Fer-1 intervention significantly restored their expression (Figure 7E, F). The animal experimental results further confirmed that MT exerted a protective effect *in vivo* by inhibiting ferroptosis, significantly reducing UVB-induced lens opacity and maintaining lens transparency, and that its effects were highly consistent with those of the ferroptosis inhibitor Fer-1.

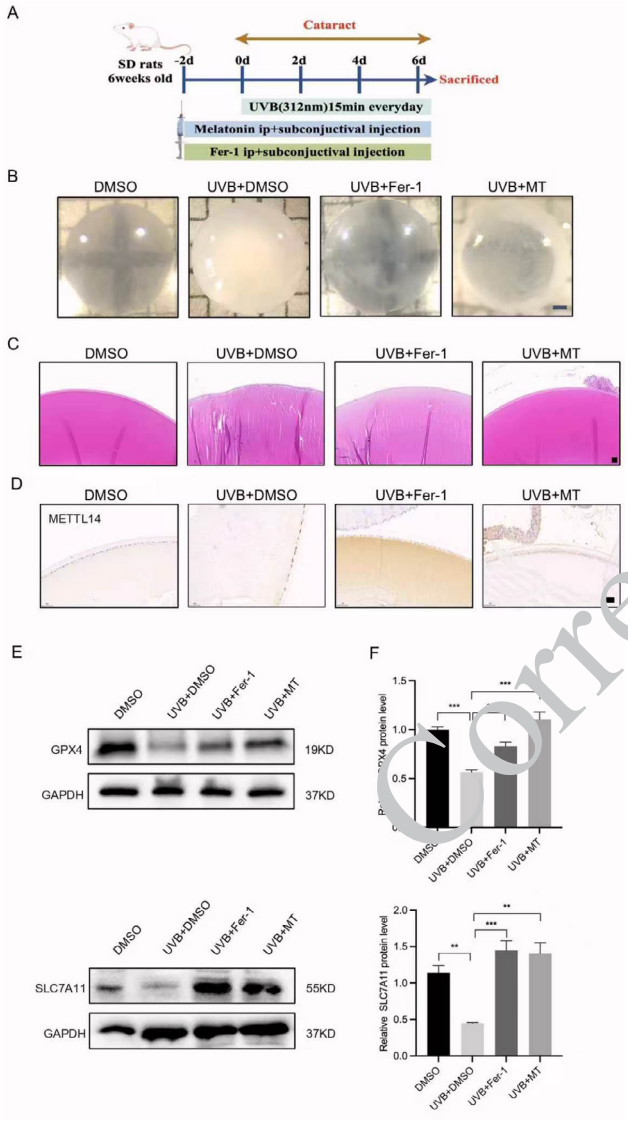

Figure 7. Melatonin (MT) restored lens transparency via suppressing ferroptosis in rats

(A) Schematic representation of the SD rat model. (B) Lenses extracted from rats and observed under a microscope. Scale bar=1 mm. (C) Total lens, Hematoxylin and eosin (HE) staining. Scale bars=50 μm. (D) Immunohistochemical (IHC) staining of METTL14 in rat lens capsules. Scale bar=50 μm. (E, F) Western blot (WB) analysis showed the protein levels of GPX4 and SLC7A11 in the lenses of the rats in each group. $^{*}P<0.05$; $^{**}P<0.01$; $^{***}P<0.001$. Data are shown as mean±SEM (n=3)SD: Sprague-Dawley; UVB: Ultraviolet B; METTL14: Methyltransferase-like 14; DMSO: Dimethyl sulfoxide; GPX4: Glutathione peroxidase 4; SLC7A11: Solute carrier family 7 member 11; DMSO: Dimethyl sulfoxide; Fer-1: Ferrostatin-1; SEM: standard error of mean

Discussion

Numerous *in vitro* and *in vivo* studies have explored the potential mechanisms of MT's protective effect against cataract formation. In *in vitro* studies, we used UVB-exposed HLECs as a model to investigate the regulatory role of MT. This model reproduced several pathological features of cataract formation, including oxidative stress, ferroptosis, and mitochondrial dysfunction. Our *in vitro* data indicated that MT inhibited ferroptosis in UVB-treated LECs by targeting METTL14, thereby reducing lipid peroxidation and restoring cellular homeostasis. Subsequently, we used a rat cataract model induced by UVB to further validate these findings. The experimental results showed that MT inhibited ferroptosis by down-regulating METTL14 expression, thereby reducing lens opacity. Both *in vivo* and *in vitro* models are frequently used in cataract research, and our results indicate that these two models are consistent with each other. Overall, our research results suggest that MT can slow the progression of cataract by inhibiting METTL14-mediated ferroptosis, providing new insights into its potential as a therapeutic strategy.

Our previous investigations revealed that the hallmarks of ferroptosis were detectable in HLEC-B3, SRA01/04, and HEK-293T cells. Although UVB irradiation induced slightly different changes in the relative expression levels of these markers across cell types, the overall trend of ferroptosis induction remained consistent. Notably, in HLEC-B3 cells, UVB was even more effective than the classical ferroptosis activator RSL3 at regulating TfR1 expression and promoting ferroptotic processes, thereby confirming UVB's strong and reliable capacity to trigger ferroptosis (6). In recent years, ferroptosis has been implicated in a wide spectrum of ocular diseases, including corneal disorders, glaucoma, retinal ischemia-reperfusion injury, and age-related macular degeneration (27-29). Growing evidence indicates that LECs are highly susceptible to oxidative stress, a central driver of cataract formation and progression (30, 31). Importantly, ferroptosis is now considered the predominant form of programmed cell death in LECs under oxidative stress conditions. Consistently, characteristic ferroptotic features—elevated ROS production, increased lipid peroxidation, and abnormal accumulation of redox-active iron—have been widely observed in the lenses of

elderly individuals and cataract patients (11). Furthermore, cataractous lenses display enhanced lipid peroxidation, reduced GPX activity, and excessive iron deposition, providing compelling evidence that ferroptosis is critically involved in cataract pathogenesis (8).

In this study, we observed that METTL14 expression was markedly up-regulated in LECs under UVB irradiation, thereby promoting ferroptosis. Conversely, silencing METTL14 attenuated UVB-induced ferroptotic cell death, suggesting that, under UVB-induced oxidative stress, METTL14 up-regulation may be a critical driver of ferroptosis in LECs. Epigenetic modifications have increasingly been recognized as key regulators of cell death and metabolic homeostasis. As a core component of the m6A methyltransferase complex, METTL14 plays essential roles in multiple biological processes, including mRNA maturation, nuclear export, metabolic regulation, and pri-miRNA processing (32-35). Emerging evidence further indicates that METTL14-mediated m6A modifications contribute to ferroptosis by modulating the stability and translation of key ferroptosis-related transcripts, including those involved in glutathione metabolism, lipid peroxidation pathways, and iron homeostasis (36). Therefore, our findings highlight a potential mechanistic link between UVB-induced METTL14 up-regulation and the exacerbation of ferroptosis in LECs, providing novel insights into the epigenetic regulation of cataract pathogenesis.

Recent ocular studies have further reported the involvement of METTL14 in models of cataract and diabetic retinopathy. Li *et al.* showed that METTL14 overexpression alleviated mitochondrial dysfunction, oxidative stress, and autophagy inhibition in high-glucose-treated LECs, and that AAV-mediated METTL14 overexpression improved lens transparency in diabetic cataract mice through m6A-dependent regulation of RPL3 (37). In contrast, Chen *et al.* reported that METTL14 was up-regulated in diabetic retinopathy rats and high-glucose-treated retinal ganglion cells, while METTL14 knockdown ameliorated retinal ganglion cell injury and diabetic retinopathy progression by reducing PHLPP2 m6A modification (38). These findings suggest that the role of METTL14 in ocular diseases may be context-dependent. In diabetic cataract, METTL14 may protect LECs through the RPL3/autophagy axis, whereas in our UVB-induced cataract model, METTL14 up-regulation promoted ferroptosis-related mitochondrial injury in LECs.

Our results demonstrate that MT suppresses UVB-induced ferroptosis in LECs by down-regulating METTL14 expression and restoring mitochondrial structure and function. *In vivo*, MT treatment significantly reduced lens opacity, alleviated oxidative stress, and partially reversed UVB-induced pathological alterations. These findings suggest that MT may represent a novel therapeutic strategy for cataract prevention and treatment through METTL14-mediated regulation of ferroptosis. Previous studies have shown that MT protects HLECs against H_2O_2-induced oxidative injury and cell death by activating the PI3K/AKT pathway (39). Beyond its antioxidant function, MT exerts multiple biological effects, including anti-nitridative, mitochondrial-protective, autophagy-modulating, anti-inflammatory, and anti-angiogenic activities, making it a versatile candidate for combating ocular diseases (20). Recent evidence further highlights the potential role of MT in cataract prevention, such as mitigating inflammation (40), reducing oxidative stress (19, 39), and alleviating anxiety-related cellular damage (41). Notably, m6A modification has emerged as a critical regulator of signaling pathways and protein functions, and accumulating studies indicate that MT can modulate m6A-dependent mechanisms in diverse contexts—for instance, attenuating LPS-induced colonic inflammation (42), delaying ovarian aging through the YTHDF2/m6A/UBE3C axis (43), and alleviating abnormal pregnancy via MTNR1B-mediated m6A regulation (44). However, whether MT directly regulates METTL14 and thereby influences LEC ferroptosis under UVB irradiation remains largely unexplored. Our study thus provides new insights into the epigenetic mechanisms of MT in cataract protection and underscores METTL14 as a potential therapeutic target.

In summary, MT effectively mitigated UVB-induced ferroptosis in lens epithelial cells by targeting METTL14-mediated lipid peroxidation, restoring mitochondrial function, and reducing oxidative stress. This mechanism offers a promising therapeutic strategy for cataract prevention and treatment.

However, a limitation of this study is that the direct molecular mechanism by which MT regulates METTL14 remains to be fully elucidated. In addition, although 500 J/m² UVB irradiation was selected as a sublethal injury dose based on LEC viability, its effects on other cell types were not directly evaluated in this study. Furthermore, we did not perform METTL14 knockdown or overexpression experiments *in vivo*; therefore, the causal role of METTL14 in the protective effect of MT against UVB-induced cataract requires further validation in animal models. Further biochemical assays, such as CETSA, SPR, and pull-down assays, are needed to confirm whether MT directly binds METTL14. Additionally, due to the lack of commercially available specific small-molecule inhibitors for METTL14, alternative pharmacological blockades could not be compared with our siRNA findings, which warrants further development of novel chemical biology tools.

Conclusion

MT alleviates cataract progression by suppressing ferroptosis in lens epithelial cells through down-regulation of METTL14 and restoration of mitochondrial function. Our study provides new insights into the role of METTL14-mediated ferroptosis in lens opacity and highlights MT as a potential pharmacological candidate for cataract prevention.

Acknowledgment

We thank www.figdraw.com for support with the flow charts in this article. This study was supported by Heilongjiang Charity Federation (Grant No. 2023HX015) and Harbin Charity Federation (Grant No. 2022HX005). The results presented in this paper were part of a student thesis.

Data Availability Statement

All animal experiments (Approval Number: No. 2023130) are approved by the Ethics Committee of the First Affiliated Hospital of Harbin Medical University, China. The data that support the findings of this study are available from the corresponding author upon reasonable request.

Authors' Contributions

H G and H L designed the study. H L, Y G, and F K conducted *in vitro* experiments; H L and J L conducted *in vivo* experiments. A Q and C Y performed statistical analyses. L S guided and supervised the study. H L, J L, and Z Y wrote the manuscript. HG revised the manuscript. All authors contributed to the submitted version of the manuscript.

Conflicts of Interest

The authors declare no conflicts of interest.

Declaration

We have not used any AI tools or technologies to prepare this manuscript.

References

1. Fukuoka H, Afshari NA. The impact of age-related cataract on measures of frailty in an aging global population. Curr Opin Ophthalmol 2017; 28: 93-97.
2. Tsentalovich YP, Verkhovod TD, Yanshole VV, Kuznetsova ID, Burnet J, *et al.* Metabolomic composition of normal aged and cataractous human lenses. Exp Eye Res 2015; 134: 15-23.
3. Cicinelli MV, Buchan JC, Nicholson M, Varadaraj V, Khanna RC. Cataracts. Lancet 2023; 401: 377–389.
4. Cooksley G, Nam MH, Nahomi RB, Rankenberg J, Smith AJO, Wormstone YM, *et al.* Lens capsule advanced glycation end products induce senescence in epithelial cells: Implications for secondary cataracts. Aging Cell 2024; 23: e14249.
5. Wei Z, Hao C, Huangfu J, Srinivasagan R, Zhang X, Fan X. Aging lens epithelium is susceptible to ferroptosis. Free Radic Biol Med 2021; 167: 94-108.
6. Mi Y, Wei C, Sun L, Liu H, Zhang J, Luo J, *et al.* Melatonin inhibits ferroptosis and delays age-related cataract by regulating SIRT6/p-Nrf2/GPX4 and SIRT6/NCOA4/FTH1 pathways. Biomed Pharmacother 2023; 157: 114048.
7. Liu H, Sun L, Mi Y, Gao Y, Luo J, Kang F, *et al.* SIRT1 prevents lens epithelial cell senescence during age-related cataract via regulating p66Shc. Aging Cell 2025; 24: e70155.
8. Dixon S J, Lemberg K M, Lamprecht MR, Skouta R, Zaitsev EM, Gleason CE, *et al.* Ferroptosis: An iron-dependent form of nonapoptotic cell death. Cell 2012; 149: 1060-1072.
9. Ma DY, Liu JX, Wang LD, Zhi XY, Luo L, Zhao JY, *et al.* GSK-3β-dependent Nrf2 antioxidant response modulates ferroptosis of lens epithelial cells in age-related cataract. Free Radic Biol Med 2023; 204: 161-176.
10. Stockwell BR, Friedmann Angeli JP, Bayir H, Bush AI, Conrad M, Dixo SJ, *et al.* Ferroptosis: A regulated cell death nexus linking metabolism, redox biology, and disease. Cell 2017; 171: 273-285.
11. Chen X, Li J, Kang R, Klionsky DJ, Tang D. Ferroptosis: Machinery and regulation. Autophagy 2021; 17: 2054-2081.
12. Li X, Guo Y, Gao R, Zhao W, Cui N. Ferroptosis in sepsis: The mechanism, the role and the therapeutic potential. Front Immunol. 2022; 13: 956361.
13. Krug RM, Morgan MA, Shatkin AJ. Influenza viral mRNA contains internal N6-methyladenosine and 5'-terminal 7-methylguanosine in cap structures. J Virol 1976; 20: 45-53.
14. Meyer KD, Saletore Y, Zumbo P, Elemento O, Mason CE, Jaffrey SR. Comprehensive analysis of mRNA methylation reveals enrichment in 3' UTRs and near stop codons. Cell 2012; 149: 1635-1646.
15. Liu Q, Gregory RI. RNAmod: An integrated system for the annotation of mRNA modifications. Nucleic Acids Res 2019; 47: W548–W555.
16. Huang H, Weng H, Sun W, Qin X, Shi H, Wu H, *et al.* Recognition of RNA N(6)-methyladenosine by IGF2BP proteins enhances mRNA stability and translation. Nat Cell Biol 2018; 20: 285-295.
17. Yin L, Ma C, Hou S, Ma X. Methyltransferase-like (METTL)14-mediated N6-methyladenosine modification modulates retinal pigment epithelial (RPE) activity by regulating the methylation of microtubule-associated protein (MAP)2. Bioengineered 2022; 13: 4773-4785.
18. Zhou J, Wan J, Gao X, Zhang X, Jaffrey SR, Qian SB. Dynamic m(6)A mRNA methylation directs translational control of heat shock response. Nature 2015; 526: 591-594.
19. Shirazi A, Haddadi H, Asadi-Amoli F, Sakhaee S, Ghazi-Khansari M, Avand A. Radioprotective effect of melatonin in reducing oxidative stress in rat lenses. Cell J 2011; 13: 79-82.
20. Crooke A, Huete-Toral F, Colligris B, Pintor J. The role and therapeutic potential of melatonin in age-related ocular diseases. J Pineal Res 2017; 63: e12430.
21. Gao Y, Liu H, Yang T, Wang J. Baicalin affects the progression of diabetic retinopathy through the RAGE/PXDN/PI3K/AKT pathway. J Transl Med 2025; 23: 95.
22. Luo J, Wei C, Sun L, Liu H, Mi Y, An Q, *et al.* Metformin attenuates lens epithelial cell senescence by suppressing cGAS-STING via SIRT1-PGC-1α-mediated mitochondrial fission. Exp Gerontol 2026; 219: 113157.
23. Meng D, Chen Y, Cui C, Huang M, Zhu J, Lu H, *et al.* Targeted delivery of avacopan via sortase A-modified extracellular vesicles attenuates endotoxin-induced retinal inflammation. Adv Healthc Mater 2026; 15: e04723.
24. Liu M, Wang J, Wang L, Yang T, Xiang F, Lu J, *et al.* The role and mechanism of asiaticoside in regulating smooth muscle cell mitochondrial Drp1 during neointimal hyperplasia and atherosclerosis. Biochem Biophys Res Commun 2026; 795: 153102.
25. Xiang F, Cui Y, Yang S, Fang Y, Wang B, Chen B, *et al.* Chronic hindlimb ischemia exacerbates ischemic stroke by disrupting cerebral hemodynamics and glycerophospholipid metabolism in mice. Sci Rep 2026; 16: 4235.
26. Liu M, Xiang F, Yang T, Sun Y, Yang J, Wang T, *et al.* Calcitonin inhibits phenotypic switching of aortic smooth muscle cells and neointimal hyperplasia through the AMP-activated protein kinase/mechanistic target of rapamycin pathway. ACS Pharmacol Transl Sci 2024; 7: 733-742.
27. Wang Y, Li P, Wang C, Wang C, Bao S, Wang S, *et al.* Lens epithelium cell ferroptosis mediated by m6A-lncRNA and GPX4 expression in lens tissue of age-related cataract. BMC Ophthalmol 2023; 23: 514.
28. Liu K, Li H, Wang F, Su Y. Ferroptosis: Mechanisms and advances in ocular diseases. Mol Cell Biochem 2023; 478: 2081-2095.
29. Hao XD, Xu WH, Zhang X, Xue J. Targeting ferroptosis: A novel therapeutic strategy for the treatment of retinal diseases. Front Pharmacol 2024; 15: 1489877.
30. Huynh TPN, Bowater RP, Wormstone IM. GSH levels serve as a biological redox switch regulating sulforaphane-induced cell fate in human lens cells. Invest Ophthalmol Vis Sci 2021; 62: 2.
31. Michael R, Bron AJ. The ageing lens and cataract: A model of normal and pathological ageing. Philos Trans R Soc Lond B Biol Sci 2011; 366: 1278-1292.
32. Owczarz M, Połosak J, Domaszewska-Szostek A, Kołodziej P, Kuryłowicz A, Puzianowska-Kuźnicka M. Age-related epigenetic drift deregulates SIRT6 expression and affects its downstream genes in human peripheral blood mononuclear cells. Epigenetics 2020; 15: 1336-1347.
33. Shan K, Zhou RM, Xiang J, Sun YN, Liu C, Lv MW, Xu JJ. FTO regulates ocular angiogenesis via a m(6)A-YTHDF2-dependent mechanism. Exp Eye Res 2020; 197: 108107.
34. Qi Y, Yao R, Zhang W, Cui Q. KAT1 triggers YTHDF2-mediated ITGB1 mRNA instability to alleviate the progression of diabetic retinopathy. Pharmacol Res 2021; 170: 105713.
35. Xu X, Cui J, Wang H, Ma L, Zhang X, Guo W, *et al.* IGF2BP3 is an essential N6-methyladenosine biotarget for suppressing ferroptosis in lung adenocarcinoma cells. Mater Today Bio 2022; 17: 100503.
36. Li L, Zeng J, He S, Yang Y, Wang C, *et al.* METTL14 decreases FTH1 mRNA stability via m6A methylation to promote sorafenib-

induced ferroptosis of cervical cancer. Cancer Biol Ther 2024; 25: 2349429.
37. Li R, Wang X, Du W, Li Q, Cui HP. METTL14 ameliorates mitochondrial dysfunction and autophagy in lens epithelial cells of diabetic cataracts via m6A modification of RPL3. Kaohsiung J Med Sci 2026; e70194.
38. Chen L, Wei T, Liu X, Cui L, Hu C, Quan Y. Methyltransferase-like enzyme 14 exacerbates retinal ganglion cell damage and diabetic retinopathy through N6-methyladenosine-dependent up-regulation of pleckstrin homology domain and leucine rich repeat protein phosphatase 2. Toxicol Appl Pharmacol 2025; 498: 117304.
39. Bai J, Dong L, Song Z, Ge H, Cai X, Wang G, *et al.* The role of melatonin as an antioxidant in human lens epithelial cells. Free Radic Res 2013; 47: 635-642.
40. Lledó VE, Alkozi HA, Sánchez-Naves J, Fernandez-Torres MA, Guzman-Aranguez A. Melatonin counteracts oxidative damage in lens by regulation of Nrf2 and NLRP3 inflammasome activity. Exp Eye Res 2022; 215: 108912.
41. Ismail SA, Mowafi HA. Melatonin provides anxiolysis, enhances analgesia, decreases intraocular pressure, and promotes better operating conditions during cataract surgery under topical anesthesia. Anesth Analg 2009; 108: 1146-1151.
42. Li Y, Ma B, Wang Z, Chen Y, Dong Y. The Effect mechanism of N6-adenosine methylation (m6A) in melatonin regulated LPS-induced colon inflammation. Int J Biol Sci 2024; 20: 2491-2506.
43. Xia W, Wang X, Li J, Zhang M, Lu J, Li H, *et al.* Melatonin mitigates ovarian aging through regulation of the YTHDF2/m6A/UBE3C axis. Acta Biochim Biophys Sin (Shanghai) 2025; 57: 1529-1538.
44. Zhao S, Dong Y, Li Y, Wang Z, Chen Y, Dong Y. Melatonin alleviates lipopolysaccharide-induced abnormal pregnancy through MTNR1B regulation of m6A. Int J Mol Sci 2024; 25: 733.